Quantum mechanical tunneling in the automerization of cyclobutadiene

R. Schoonmaker, T. Lancaster, and S. J. Clark

Citation: The Journal of Chemical Physics **148**, 104109 (2018); doi: 10.1063/1.5019254
View online: https://doi.org/10.1063/1.5019254
View Table of Contents: http://aip.scitation.org/toc/jcp/148/10
Published by the American Institute of Physics

Quantum mechanical tunneling in the automerization of cyclobutadiene

R. Schoonmaker, T. Lancaster, and S. J. Clark
Department of Physics, Durham University, South Road, Durham DH1 3LE, United Kingdom

(Received 12 December 2017; accepted 21 February 2018; published online 12 March 2018)

Cyclobutadiene has a four-membered carbon ring with two double bonds, but this highly strained molecular configuration is almost square and, via a coordinated motion, the nuclei quantum mechanically tunnels through the high-energy square state to a configuration equivalent to the initial configuration under a 90° rotation. This results in a square ground state, comprising a superposition of two molecular configurations, that is driven by quantum tunneling. Using a quantum mechanical model, and an effective nuclear potential from density functional theory, we calculate the vibrational energy spectrum and the accompanying wavefunctions. We use the wavefunctions to identify the motions of the molecule and detail how different motions can enhance or suppress the tunneling rate. This is relevant for kinematics of tunneling-driven reactions, and we discuss these implications. We are also able to provide a qualitative account of how the molecule will respond to an external perturbation and how this may enhance or suppress infra-red-active vibrational transitions. *Published by AIP Publishing.* https://doi.org/10.1063/1.5019254

INTRODUCTION

The motions and locations of nuclei underpin how we define molecular structure, structural transitions, and chemical reactions. Cyclobutadiene as a free molecule exhibits nuclear delocalization that determines the point group symmetry, for although the lowest-energy electronic configuration suggests that the molecule is rectangular with two double and two single bonds, the molecule automerizes via nuclear tunneling, which results in an overall square symmetry.[1–3] While this automerization is similar to a reaction, since it involves the motion of nuclei to a different structural conformation, it is distinct since the reactant is chemically identical to the product and the transition does not require thermal or collision processes.[4] These distinctive qualities therefore present an opportunity to study how a structure changes when nuclei tunnel, without additional complications such as dynamic molecular collisions. Here we calculate the energy eigenstates of the nuclear motion that correspond to active infra-red (IR) excitations and their corresponding nuclear wavefunctions. With these wavefunctions, we are able to describe and explain how the different motions of the molecule can enhance or suppress the rate of tunneling.

There are two electronic configurations at low energies in cyclobutadiene, a singlet state and a triplet state.[5] Historically it was unclear which state was most important in the low temperature behaviour of cyclobutadiene.[6] While it was found that a D_{2h} singlet state has the lowest energy,[4,5] the electronic structure of the triplet state remains of considerable interest due to the conflicting accounts of the aromatic stabilization or antiaromatic destabilization and the role of ring strain in the electronic structure.[7–10] At low temperatures, the molecule tunnels between two D_{2h} singlet configurations,[1,11] and theoretical studies of this automerization suggest that a D_{4h} triplet state may determine the effective height of the reaction barrier.[12–14] However the precise structural configuration where the energies of the singlet and triplet state are equivalent is not known,[15] if it exists at all.[16,17] Additionally in the free molecule, the strength of the spin-orbit interaction, which permits a transition between the singlet and triplet electronic states, is small in comparison to the kinetic energy of the nuclei,[18] and this will suppress the transition between the singlet and triplet states. In this work, we therefore assume that singlet-triplet transitions are symmetry-forbidden, so only singlet states will be considered for tunneling through the intermediate D_{4h} structural configuration.

Some theoretical studies of tunneling in the singlet ground state focus on the energetic surface and barrier height of this nuclear tunneling process, as these are required to calculate the tunneling rate.[13,16,19,20] In chemical systems, the most straightforward approaches to calculate tunneling rates use WKB(J) formalism;[14,21,22] however, this formalism requires that reverse-tunneling processes are negligible. There is therefore reason to doubt its applicability in the case of cyclobutadiene, where the two configurations are symmetry-equivalent and reverse tunneling can readily occur. Another common method of calculating rates uses instantons[23] which can be used to map the system onto a one-dimensional tunneling problem.[24,25] However as the nuclear potential is anharmonic in cyclobutadiene, it is likely that an instanton-based model will not be able to accurately reproduce the tunneling rate and other properties, such as the motion of the hydrogen nuclei, which is dependent on wavefunction configurations different from those on the instanton path.

The other theoretical work focuses on the determination of the Raman spectrum of the molecule that is important to recognize and classify the experimental Raman response of the molecule.[26,27] Due to time evolution's dependency on the Hamiltonian, the calculations of the Raman spectrum and the tunneling rate in this single-molecule system are equivalent and it is possible to study tunneling under a Hamiltonian framework.[2,26]

The behaviour of interest to this work is tunneling between cyclobutadiene's rectangular configurations. This tunneling results in a small correction, where each of the known Raman peaks that have been previously classified under a rectangular symmetry divides into pairs. A previous study by Čársky *et al.*[26] used a three-dimensional Taylor expansion on a potential calculated under the generalized valence bond method, to approximate the wavefunction and to calculate the energy separation of these pairs. Unfortunately the energy separation that they predicted was not experimentally observed when cyclobutadiene was bound in a solid matrix, possibly due to the environmental breaking of the square symmetry.[3,28]

In this paper, we propose a general method for calculating the energy eigenstates and wavefunctions of nuclei bound in molecules based on an effective potential energy surface determined by the electrons and Coulombic forces. We use this to calculate the Raman spectrum and molecular wavefunctions using the symmetry-conserving motions permitted under the rectangular symmetry. We are able to determine how the nuclear motions for different Raman resonance states affect the rate of tunneling. We show how the calculation and interpretation of the wavefunction reveal the sensitivity of the system to environmental effects and how the inclusion of hydrogenic motion affects the carbon motion and the strength of the tunneling interaction.

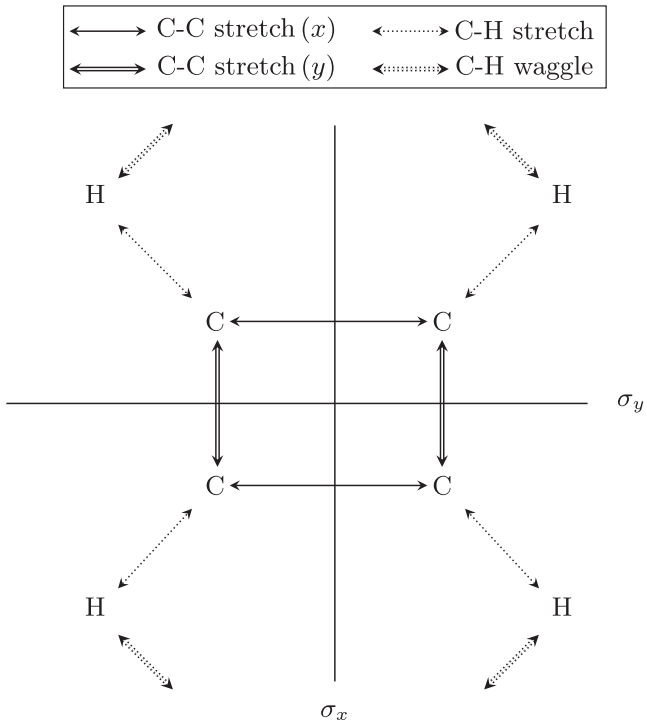

FIG. 1. The (rectangular) a_g motions permitted in cyclobutadiene: C–C and C–H bond stretches and the C–H bond waggle. The σ_x and σ_y reflection symmetries are also shown.

METHODS

Assuming adiabatic separation between electrons and nuclei, we consider the four in-plane (rectangular, D_{2h}) a_g symmetry-preserving motions of the molecule, as shown in Fig. 1. This assumes that the effective potential, which is a function of the nuclear positions, can be expressed as a sum of potentials. Each of these potentials is related to a particular symmetry operator and is a function of only those nuclear coordinates that break that particular symmetry.[29,30] This effectively assumes that the motion in each of these symmetry directions is independent and permits us to decouple the symmetry-breaking and symmetry-conserving motions. The Hamiltonian for this system is therefore

$$\mathcal{H} = \frac{\mathbf{p}_\mathrm{C}^\dagger \cdot \mathbf{p}_\mathrm{C}}{2m_\mathrm{C}} + \frac{\mathbf{p}_\mathrm{H}^\dagger \cdot \mathbf{p}_\mathrm{H}}{2m_\mathrm{H}} + V_\mathrm{eff}(\mathbf{r}_\mathrm{H}, \mathbf{r}_\mathrm{C}), \tag{1}$$

where $\mathbf{r}_\mathrm{C}$ and $\mathbf{r}_\mathrm{H}$ are the displacements of the carbon and hydrogen atoms from the centre of mass, respectively, and m_C and m_H are the effective masses of the carbon and hydrogen atoms that are determined by the concerted motion of the nuclei, respectively, both being four times the value of the natural masses of the nuclei. Here V_eff is the effective potential determined by the adiabatically separated electrons, and the nuclear momentum operators defined in the usual way[21] with the canonical commutation relations $[\mathbf{p}_\mathrm{H} \cdot \mathbf{e}_i, \mathbf{r}_\mathrm{H} \cdot \mathbf{e}_j] = -\mathrm{i}\hbar\delta_{ij}$, $[\mathbf{p}_\mathrm{C} \cdot \mathbf{e}_i, \mathbf{r}_\mathrm{C} \cdot \mathbf{e}_j] = -\mathrm{i}\hbar\delta_{ij}$, where $\mathbf{e}_0$ and $\mathbf{e}_1$ are a pair of two-dimensional perpendicular unit vectors. However, calculation in this basis is inconvenient because there are large regions of $\mathbf{r}_\mathrm{H}$ which can be effectively ignored. Additionally a good basis choice is convenient for the interpretation of results, and so we choose a new basis for the calculation, as shown in Fig. 2. This coordinate transformation results in a transformed set of canonical momenta that are related by $\mathbf{p}_\mathrm{C} = \mathbf{p}'_\mathrm{C} - \mathbf{p}'_\mathrm{CH}$ and $\mathbf{p}_\mathrm{H} = \mathbf{p}'_\mathrm{CH}$. The Hamiltonian becomes

$$\mathcal{H} = \frac{\mathbf{p}_\mathrm{C}'^\dagger \cdot \mathbf{p}'_\mathrm{C}}{2m_\mathrm{C}} - \frac{\mathbf{p}_\mathrm{C}'^\dagger \cdot \mathbf{p}'_\mathrm{CH} + \mathbf{p}_\mathrm{CH}'^\dagger \cdot \mathbf{p}'_\mathrm{C}}{2m_\mathrm{C}} + \frac{m_\mathrm{C} + m_\mathrm{H}}{m_\mathrm{C} m_\mathrm{H}} \mathbf{p}_\mathrm{CH}'^\dagger \cdot \mathbf{p}'_\mathrm{CH} + V_\mathrm{eff}. \tag{2}$$

This basis choice reflects the structure of the molecule, which is determined by V_eff. The potential is four dimensional, however, because of the structure we are in practice able to subdivide the potential into three terms that reflect the potential energy of the C–C ring or the C–H bond, and the cross terms

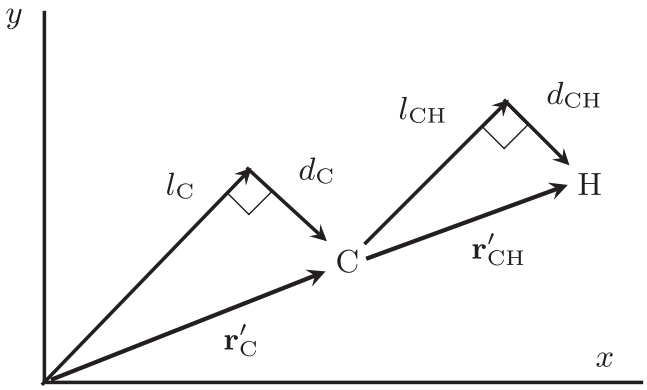

FIG. 2. The calculation basis $\mathbf{r}'_\mathrm{CH} = (d_\mathrm{CH}, l_\mathrm{CH})$ and $\mathbf{r}'_\mathrm{C} = (d_\mathrm{C}, l_\mathrm{C})$ used here, shown on a single quadrant of the molecule. This new coordinate set is related to the absolute positions by $\mathbf{r}'_\mathrm{CH} = \mathbf{r}_\mathrm{H} - \mathbf{r}_\mathrm{C}$ and $\mathbf{r}'_\mathrm{C} = \mathbf{r}_\mathrm{C}$.

between them. We use

$$V_{\text{eff}} = V_1(\mathbf{r}'_{\text{C}}) + V_2(\mathbf{r}'_{\text{CH}}) + V_3(\mathbf{r}'_{\text{C}}, \mathbf{r}'_{\text{CH}}), \quad (3)$$

$$V_1(\mathbf{r}'_{\text{C}}) = V_{\text{eff}}(\mathbf{r}'_{\text{C}}, \mathbf{R}_{\text{CH}}), \quad (4)$$

$$V_2(\mathbf{r}'_{\text{CH}}) = V_{\text{eff}}(\mathbf{R}_{\text{C}}, \mathbf{r}'_{\text{CH}}), \quad (5)$$

where the coordinates $\mathbf{R}_{\text{CH}}$ and $\mathbf{R}_{\text{C}}$ are the chosen such that $V_{\text{eff}}(\mathbf{R}_{\text{C}}, \mathbf{R}_{\text{CH}})$ is the global minimum of the potential. The potential $V_3(\mathbf{r}'_{\text{C}}, \mathbf{r}'_{\text{CH}})$ is the four-dimensional correction term that accounts for the coupled nature of the bonding. If we have chosen the basis well then $V_3(\mathbf{r}'_{\text{C}}, \mathbf{r}'_{\text{CH}})$ is small everywhere, and we can qualitatively characterize the molecule as a simple combination of C–C and C–H bond motions, in a form analogous to the harmonic approximation.[29,30]

The choice of this basis also enables us to impose appropriate boundary conditions on the system. A pair of potential cutoffs $V_1^{\max}$, $V_{2,3}^{\max}$ was chosen so that in the calculation only regions $V_1(\mathbf{r}'_{\text{C}}) < V_1^{\max}$ and $V_2(\mathbf{r}'_{\text{CH}}) + V_3(\mathbf{r}'_{\text{C}}, \mathbf{r}'_{\text{CH}}) < V_{2,3}^{\max}$ are included. A potential cutoff is appropriate as regions outside the boundary have a too high potential energy and so have a negligible amplitude contribution to the wavefunction and energy. We make two different choices of potential cutoff since the carbon and hydrogen nuclei have very different masses and different amounts of potential energy.

To perform the calculation, the coordinate space was divided into a Cartesian mesh. Values of the mesh spacing in each dimension and the potential cutoffs $V_1^{\max}$ and $V_{2,3}^{\max}$ were set so that the energy of the 2nd excitation from the ground state, which is the lowest energy IR vibration, was converged to one part in 30. This corresponded to 38 000 points. This corresponded to a convergence of tunneling separation energies to one part in 4, and due to the coarseness of the grid around the barrier and the rapid change of the wavefunction in this region, they are likely 20% smaller. The ratios between tunneling separation energies were converged to one part in 40, so although the total separation energies are not well converged, their relative sizes are. This allows us to compare the strength of tunneling between different vibration states. The eigenvalues were calculated using the dqds (differential quotient difference with shifts) algorithm,[31] and the eigenvectors were calculated using Relatively Robust Representations (RRR),[32] as implemented in the LAPACKE library.[33]

The potential $V_{\text{eff}}(\mathbf{r}_{\text{C}}, \mathbf{r}_{\text{CH}})$ was calculated with density functional theory (DFT). This was performed using the plane-wave code CASTEP.[34] As plane-wave code relies on a periodic basis set, the size of the unit cell and the cutoff energy of the plane waves were converged, to where the error in the barrier height energy was less than 0.9 meV. The exchange correlation correction was calculated using the local density approximation (LDA).[35]

RESULTS

DFT calculations found that when the potential is separated into V_1, V_2, and V_3 terms, the range of V_3 never exceeded 10% of the energetic variation from the global potential minimum, and there was no discernible change in the position of the minimum of $V_2(\mathbf{r}'_{\text{CH}}) + V_3(\mathbf{r}'_{\text{C}}, \mathbf{r}'_{\text{CH}})$. This will permit us to qualitatively interpret the results as linearly linked C–H and C–C bond motions. We find the V_1 potential, for which a cross section is shown in Fig. 3, to be very similar to the standard one-dimensional (1D) double well system, in which the first few energy levels are well localized. As their energy is less than the barrier height, their wavefunctions tunnel through the central barrier. The characteristic features of localized states in the double well are that they are found in closely energetically spaced symmetric/antisymmetric pairs and that the tunneling rate across the barrier is proportional to this energy separation of the pairs. The more localized these states are, the smaller the energy separation between these pairs is, and correspondingly the smaller the rate of tunneling is. We performed computations on the two-dimensional potential as well as the four-dimensional potential, to compare how motion of the hydrogen nucleus affects the tunneling of the carbon ring.

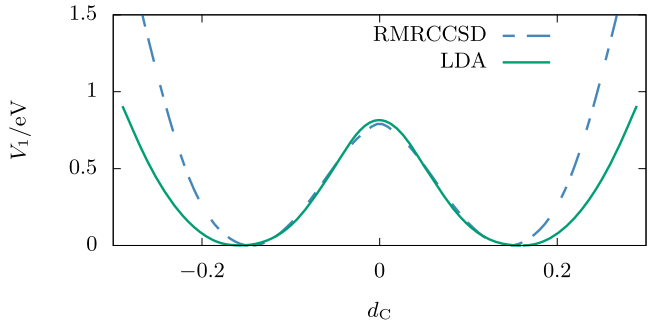

FIG. 3. The potential $(\mathbf{r}'_{\text{C}})$ shown for a constant l_{C} chosen such that the potential energy at $\mathbf{r}'_{\text{C}} = (0, l_{\text{C}})$ is minimized. Potentials calculated using LDA here ($l_{\text{C}} = 2.02$), and calculations of reduced multireference coupled-cluster method with singles and doubles (RMRCCSD) ($l_{\text{C}} = 2.07$) taken from Ref. 27 are compared.

Restricted 2D calculations

In order to understand how the multidimensional nature of the system affects the tunneling rate, we performed calculations on two two-dimensional (2D) subsystems in addition to the full 4D case. The 2D calculations were performed, where either $V_2 + V_3 \equiv 0$ (called ring-only) or $V_1 + V_3 \equiv 0$ (called C–H-only). The results for the C–H-only calculation are straightforward as unlike V_1 there is only one potential well that is predominantly harmonic. The V_2 potential and wavefunctions are shown in Fig. 4. There are two principal excitations, which we define as those states in which there is only one node in the wavefunction, as these correspond to the experimentally observable Raman excitations from the ground state. These states will dominate the spectrum since the wavelength of infrared radiation is much longer than the size of the molecule, so the gradient of a resonant electric field is roughly constant and states with multiple wavefunction nodes will generate a smaller response. These principal excitations are fairly conventional with both the waggle mode, where the wavefunction node is aligned along l_{CH} shown in Fig. 4(c), and the stretch mode, in which the wavefunction mode is aligned along d_{CH} shown in Fig. 4(b). The energies in Table I show that the waggle mode has a lower energy than the stretch mode, due to the shape of the potential as the C–H

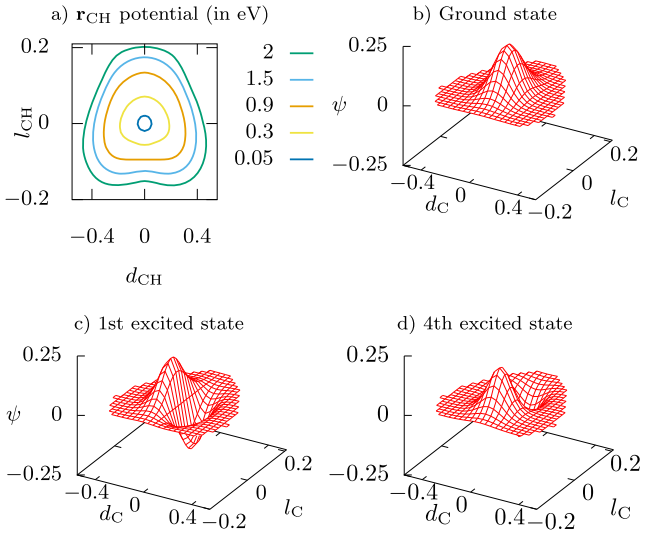

FIG. 4. (a) The governing potential $V_2(\mathbf{r}_{CH})$. (b)–(d) Wavefunctions of the principal excited states with fixed $\mathbf{r}_C$ so that V_1 is at a minimum. ψ is the unitless finite (and real) wavefunction and defined so that the sum over the points (located at line intersections) $\sum\psi^2 = 1$.

bond is stiffer with respect to length changes than to lateral changes.

The V_1 potential used for the ring only calculation is shown in Fig. 5. The shape of the potential is analogous to a two dimensional version of the double well potential as shown in the cross section of Fig. 3. Compared to the coupled-cluster calculations, the LDA potential used here has a similar barrier shape and height but has wider wells.[27] Comparatively this will lead to a reduced localization of the wavefunction and weaker tunneling than if a coupled-cluster potential was used. The contours around the two wells of the V_1 potential in Fig. 5 resemble a pair of egg-shaped ovals, and the effects of the single and double electronic bonds are visible. The long direction of each oval is aligned with the single bond, and the short width of the oval is aligned with the double bond. The wavefunctions for the lowest six energy states shown in Fig. 6 are the principal

TABLE I. Energies of eigenstates calculated under ring-only and C–H only constraints. States are labeled by energy hierarchy and rectangular symmetry considerations (D_{2h}). For the ring-only case, the energy separation between symmetric and antisymmetric states is also shown.

Ring only			
State	D_{2h}	Energy (cm^{-1})	TSE (cm^{-1})
0 and 1	Ground	0	0.0008
2 and 3	$1A_g$	1067	0.112
4 and 5	$2A_g$	1611	0.112

C–H only		
State	D_{2h}	Energy (cm^{-1})
0	0	0
1	$1A_g$	1248
2	$1A_g^2$	
3	$1A_g^3$	
4	$2A_g$	3139

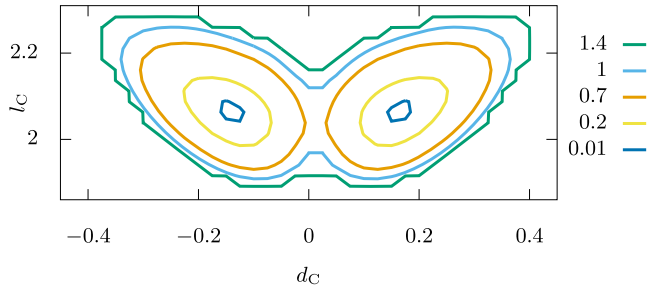

FIG. 5. The governing potential $V_1(\mathbf{r}'_C)$, the energies of the potential are in eV. The jagged edge at 1.4 eV chosen as the boundary of DFT calculation, above the 1.13 eV cutoff.

excitation states. These need to be defined slightly differently to the C–H bond case since there are no calculations in which there is a single continuous wavefunction node, as it continues past the potential cutoff in the calculation. We define the principal excitation states here as the states in which there is only one wavefunction node in each potential well. Due to the anharmonicity of the potential, the existence of multiple nodes does not suppress the Raman response. This is because in anharmonic systems under the perturbation of a linear spatial potential, the ground state can transition to a multiple node wavefunction, as the sum of the raising and lowering operators $\hat{a}^\dagger + \hat{a}$ is not proportional to the position operator $\hat{x}$. The wavefunctions show that the single and double bonds give rise to these principal excitations, with those corresponding to the length-excitation with the wavefunction node across the short axis of the oval [Figs. 6(c) and 6(d)] and those corresponding

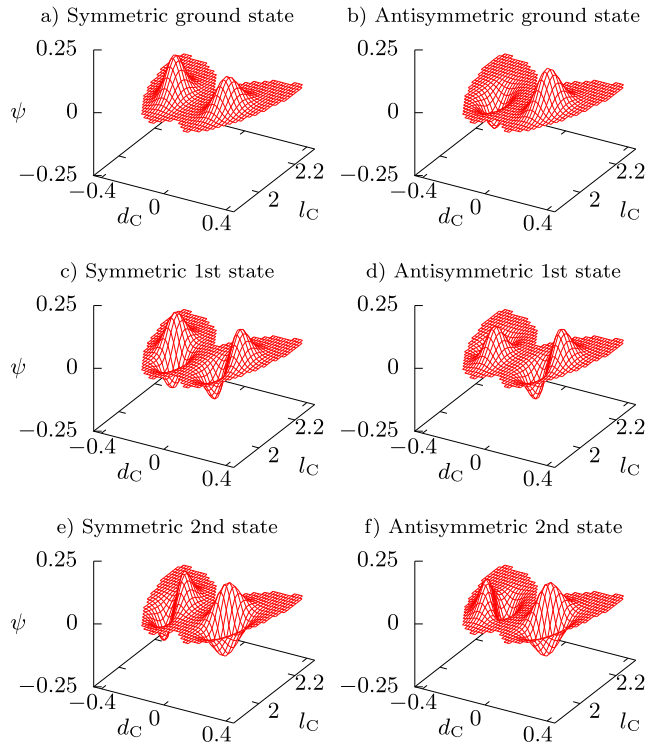

FIG. 6. (a)–(f) Real wavefunctions of the finite 2D system with fixed $\mathbf{r}_{CH}$ so that $V_2 = 0.0$, with the first three (rectangular) states and their symmetric/antisymmetric pair. Values of ψ are normalized over the sum of their squares; all coordinates l_C and d_C are in Angstroms. (a) and (b) correspond to the ground state under rectangular considerations, (c) and (d) correspond to the long-bond excitation, and (e) and (f) correspond to the short-bond excitation.

to the width excitation with the wavefunction node along the long axis [Figs. 6(e) and 6(f)].

The six lowest-energy states are shown in Table I. They are found in symmetric/antisymmetric pairs and are separated by a small energy which we call the tunneling separation energy (labeled TSE). Within each pair, the wavefunction density, the square of the wavefunction, is very similar and differs significantly only in the tunneling region between the two wells. By contrast, in this region, the wavefunction phase either stays the same (symmetric states) or changes sign (antisymmetric states). In each pair, the symmetric state is of lower energy than the antisymmetric state, in the low energy states that we calculated. By analogy to the double well, the differences in energy between each state in the pair give the rate of tunneling for these states. These energy differences, shown in Table I, determine the tunneling rate. The greater the energy difference between the pair, the higher the tunneling rate. This is because a localized state constructed from a superposition of the symmetric/antisymmetric states will oscillate between the wells at a frequency $f = \Delta E/\hbar$, which increases as energy separation ΔE. As expected, the pair splitting increases with respect to the total state energy, but this relationship is not linear; the length and width excitations both have around the same tunneling separation energies despite the difference in the total energies. This is because the motion and the momentum in the short-bond are more tangentially aligned to the barrier, and so the wavefunction does not penetrate so far through it.

To summarise, in the two-dimensional calculations, we find that in the C–H-only calculations the bond motion is very similar to the archetypal C–H bond, with a high energy stretch mode of energy around 3100 cm^{-1} and a low energy waggle mode.[30] In the ring-only calculations, we find that the potential reflects the long and short bonds determined by the electrons and these two bonds are responsible for the two different vibrational excitation energies. The system behaves similarly to a 1-D double well as states are found in symmetric/antisymmetric pairs, but the energy of a vibrational state is

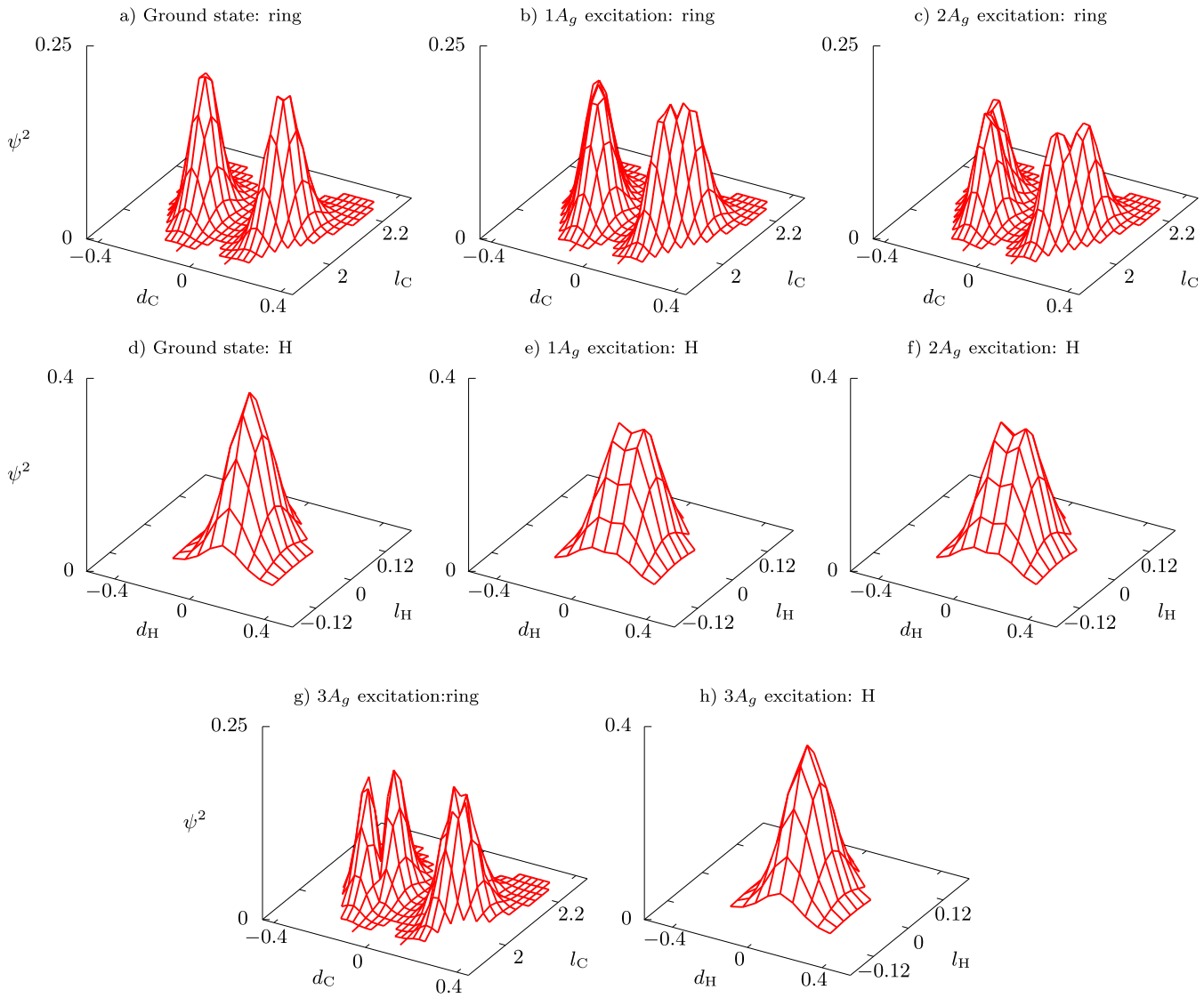

FIG. 7. Pairwise average of the wavefunction densities of the first three principal rectangular excitations projected onto (a)–(c) the ring coordinates and (d)–(f) hydrogenic coordinates, and the fourth principal rectangular excitation projected onto (g) ring coordinates and (h) hydrogenic coordinates. Coordinate distances are in Å, and the densities normalized over the grid.

not enough to determine the tunneling, as the distribution of the momentum is also important.

4D calculations

When we consider the hydrogenic and carbon-ring motions together, there are four principal excitations possible from D_{2h} symmetry considerations and the ground state.[36] The most important effect of coupling the hydrogen and ring systems together is a mixing of the motions. As a result, the hydrogen and carbon motions become correlated and illustrative sketches of these correlated motions are shown in Fig. 8.

Of these, the ring motions and the C–H waggle mix the most strongly and form three different states. The C–H stretch motion only weakly couples with the ring motion, and as a result, the energy is very similar to the C–H stretch calculated in the two-dimensional case. This can be seen from the projected densities, defined as $\rho_{\mathrm{CH}}(\mathbf{r}_{\mathrm{CH}}) = \sum_{\mathbf{r}_{\mathrm{C}}} \psi(\mathbf{r}_{\mathrm{C}}, \mathbf{r}_{\mathrm{CH}})^2$ and $\rho_{\mathrm{C}}(\mathbf{r}_{\mathrm{C}}) = \sum_{\mathbf{r}_{\mathrm{CH}}} \psi(\mathbf{r}_{\mathrm{C}}, \mathbf{r}_{\mathrm{CH}})^2$, shown in Fig. 7; since the wavefunctions' nodes do not pass through the four-dimensional space perpendicular to either the hydrogenic coordinates or the ring coordinates, there are no nodes where the density falls to zero in any of the density projections. Most importantly, the density is still split into two regions on either side of the central barrier and this corresponds to a small energy separation between the symmetric and antisymmetric pair. This means that along with the correlations between hydrogenic and carbon-ring motions, the excited states are well localized into the rectangular states.

The first two excited states, $1A_g$ and $2A_g$ shown in Figs. 7(b), 7(e), 7(c), and 7(f), are the results of strong mixing between the C–H waggle and the long-bond excitation in the ring. By comparison, the $1A_g$ excitation is broader and mixes more strongly. This can be observed since while in both excitations there is a saddle point between the two density maxima, which are present in both H and ring motions. In the $1A_g$ excitation, the density at the saddle point is more similar to the density at the maxima than that in the $2A_g$ excitation. This is likely because the carbon and hydrogen nuclear movements are mixed and must share the limited energy available in the state. This means that they are constrained to remain near the minima in the potential. The $3A_g$ excitation mostly comprises the short bond excitation in the ring and is accompanied by a much smaller amount of hydrogen motion than for the other excitations, as the projected density for the hydrogen is very similar to that of the ground state.

However the projected densities do not provide important information on correlations of the nuclear motion in the excited states. While they show how much the hydrogenic and carbon motions have combined, they do not show how the motions are correlated. This information is required to match the states with schematic motions in Fig. 8. It is given by the expectation function

$$\langle d_{\mathrm{CH}}(\mathbf{r}_{\mathrm{C}})\rangle = \frac{\sum_{\mathbf{r}_{\mathrm{CH}}} d_{\mathrm{CH}}\psi(\mathbf{r}_{\mathrm{CH}}, \mathbf{r}_{\mathrm{C}})^2}{\sum_{\mathbf{r}_{\mathrm{CH}}} \psi(\mathbf{r}_{\mathrm{CH}}, \mathbf{r}_{\mathrm{C}})^2}, \tag{6}$$

which calculates the expected position of the hydrogen for a choice of ring coordinates. This is shown in Fig. 9. Using this, we are able to obtain the correlated motions of the atoms. In the

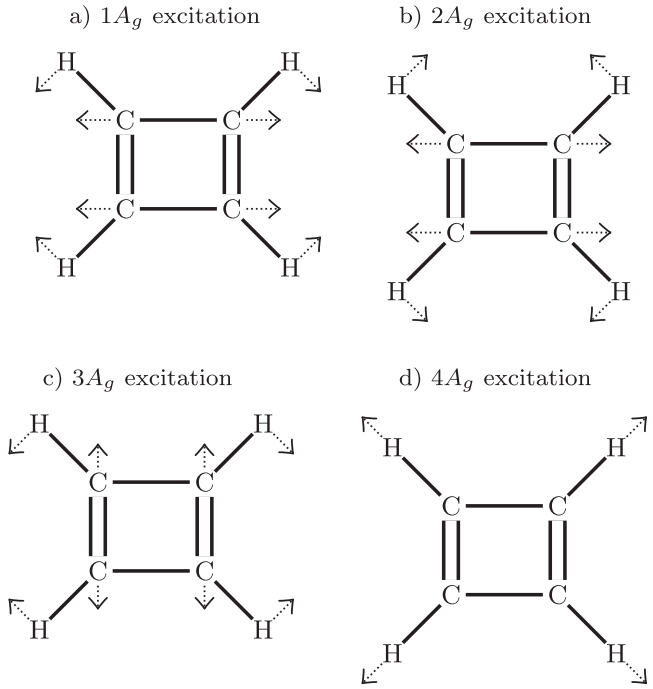

FIG. 8. A_g excitations in cyclobutadiene.

$1A_g$ excitation, when the long bond is stretched, the hydrogen waggles in the same direction. The two are positively related, and so the hydrogen waggle and long-bond stretch are in phase. The $2A_g$ is the reverse situation, and so the motions are instead out of phase. In the $3A_g$ excitation, there is less movement overall in the C–H waggle, but the short-bond excitation and the waggle motion are also out of phase. In the $2A_g$ excitation, there is a sharp change in the hydrogen displacement at $d_{\mathrm{C}} = 0$ accompanied by a sign change in $\langle d_{\mathrm{CH}}\rangle$; this is possible without the energetic penalty associated with a rapid change in the wavefunction because the wavefunction amplitude here is so low.

These calculations are able to evaluate the energies and wavefunctions of nuclear energy states which can be used to calculate all the properties of the excited states. However, to perform this calculation effectively, and in order to interpret the results, the coordinate system used needed to reflect the structure of the potential energy surface. Since the potential energy surface is determined by the electrons, we are able to use the bond lengths and angles (or the inter-atomic distances) as this basis. It is also important to restrict the space of the calculation, and this can be done by an appeal to the structure of the potential energy surface. It is important to ensure that the curvature of the wavefunctions, determined by the width of the well and the effective mass of the system in the chosen coordinates, is captured effectively. While this is done by choosing appropriate potential energy cutoffs and a choice of mesh grid spacing, the unequal curvature of the wavefunctions in Figs. 9, 4, and 6 suggests that improvements could be made, which would further reduce the size and complexity of the computation.

In the ring-only vibrations (detailed in Table I), the inclusion of the hydrogenic motion (detailed in Table II) suppresses tunneling motion in long-bond excitation states but enhances it in the short-bond excitation states. This is in contrast to

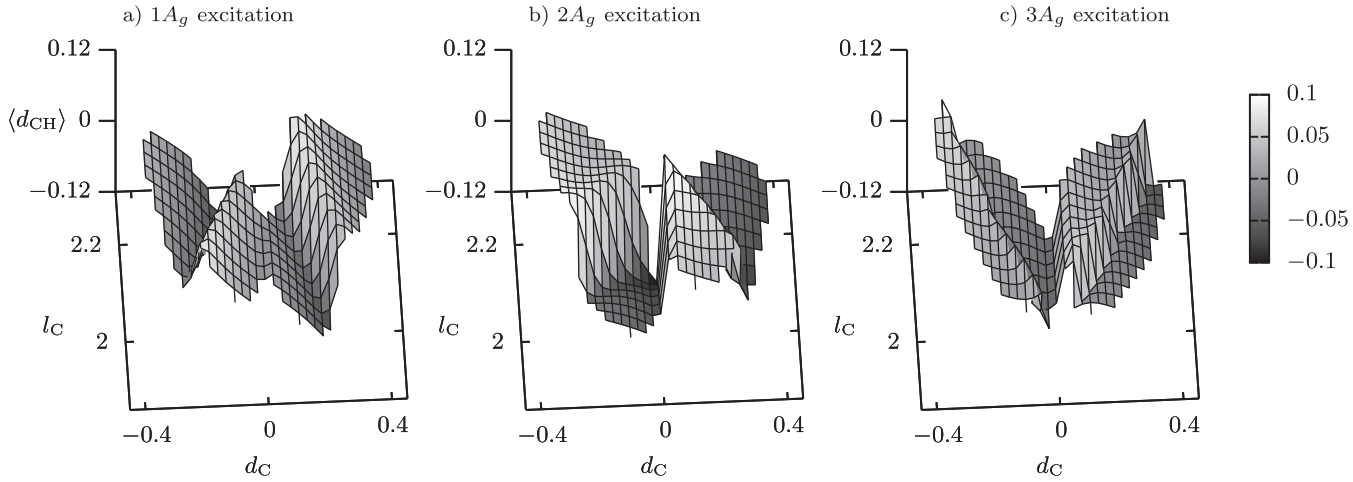

FIG. 9. The expectation function $\langle d_{CH}(\mathbf{r}_C) \rangle$, which shows how the hydrogen and carbon motions are correlated. The values of all axes are in Angstroms.

the two-dimensional results, in which the tunneling rate is equal for both single and double-bond stretches. There are two causes for difference in the tunneling rate as more degrees of freedom are considered: in the $1A_g$ excitation, the combination of hydrogen motion with the long bond stretch lowers the energy of the vibration from 1067 cm^{-1} to 839 cm^{-1}; this lower energy results in a reduction of the nuclear momentum and the tunneling energy difference from 0.112 cm^{-1} to 0.074 cm^{-1}. The second is caused by correlations between the carbon and hydrogen nuclei that suppress the tunneling rate. For the $3A_g$ out-of-phase waggle state shown in Fig. 9(b), as the ring conformation approaches $d_C = 0$, $\langle d_{CH} \rangle$ remains high, and at $d_C = 0$ there is a sharp change in $\langle d_{CH} \rangle$. This means that when the ring is in a conformation that is conducive to tunneling, the hydrogen is out of place, and so the tunneling rate is suppressed for this vibrational mode. Based on this analysis, the deuterated molecule due to an increased mass would have smaller transition frequencies and lower tunneling rates for all the states, and we find this to be the case in related calculations.

TABLE II. Energies and the tunneling separation energy (TSE) between symmetric/antisymmetric pairs of eigenstates ranked by energy and classified with D_{2h} symmetry considerations in the full 4-dimensional calculation. Principal excitations that we expect to dominate the Raman spectrum are marked with a star. A large number of states are not presented. Since they are not principal excitations, they are unconverged. Due to this, the state numbers of the final two excitations are likely incorrect.

States	D_{2h} *label*	Energy (cm^{-1})	TSE (cm^{-1})
0 and 1	Ground	0	0.025
2 and 3*	$1A_g$	839	0.074
4 and 5*	$2A_g$	1005	0.046
6 and 7*	$3A_g$	1481	0.26
8 and 9	$1A_g^2$	1661	0.13
10 and 11	$1A_g \times 2A_{1g}$	1811	0.14
12 and 13	$2A_g^2$	1980	0.057
...			
...			
28 and 29*	$4A_g(+)$	3073	0.13

SYMMETRY AND RAMAN EXCITATIONS

Point group symmetries are used to classify and assign the eigenstates of nuclear motion;[29,30] however, in cyclobutadiene, the symmetry of the molecule is ambiguous. This is because there are two equivalent minima in the potential energy surface, at nuclear configurations that correspond to a D_{2h} symmetry, but tunneling means that the eigenstates of the system are superpositions of these two configurations with a D_{4h} symmetry. Additionally the typical energies of the tunneling separation are small enough that they may be distorted by an external perturbation, so we give an account for how this can occur as well.

In harmonic systems, only excitations from the ground state to eigenstates with single nodes (principal transitions) are easily observable. Point group symmetries are useful for such systems as they allow us to predict the number of, and symmetry of, these principle transitions.[36] When we treat cyclobutadiene as a molecule with D_{2h} symmetry, this theory predicts that our calculations will accommodate four principle transitions of A_g symmetry. When we treat it with D_{4h} symmetry, it is predicted that there are two principle transitions with a A_{1g} symmetry and two with B_{2g} symmetry. This conflicts with our results, which show ten eigenstates arranged in pairs of similar energy, corresponding to up to nine principle transitions. The discrepancy between these two models is due to the anharmonicity of the potential. While D_{4h} is a higher symmetry, the lowest energy nuclear configuration of D_{4h} symmetry is in fact a saddle point rather than a minimum, so the requirement for this type of treatment, that the potential is harmonic, is not satisfied.

Since this anharmonicity is most significant in the V_2 potential, it is instructive to re-examine the 2D wavefunctions of Fig. 6. All of these states satisfy D_{4h} symmetry: symmetric states correspond to A_{1g} motions and the antisymmetric states to B_{2g} motions. However most of the wavefunction is localised around the energetic minima located at configurations of D_{2h} symmetry, and around which the potential is almost harmonic. From the energies in Table I, the effective width of the potential barrier at the D_{4h} symmetry point is high enough that the tunneling separation energies are much less than the energies

of the lowest energy eigenstates. This means that for energetic purposes, superpositions of configurations around the two minima in the potential are well separated and only interact weakly, and the coarse structure of the spectrum (in which the symmetric/antisymmetric pairs are treated as single eigenstates) can be readily interpreted using a D_{2h} symmetry approach that relies on harmonicity.[26,27] The overall D_{4h} symmetry is therefore only relevant for an experiment sensitive to the tunneling separation energy, or for high-energy excitations that can tunnel through the barrier more easily. This is similar to the inversion doubling of spectral peaks, for example, in ammonia.[37,38]

Anharmonicity and symmetry are of further relevance to calculations of cyclobutadiene. In particular, we made the assumption that the different symmetry breaking and conserving motions could be decoupled. However recent calculations[39,40] found metastable configurations of similar energy to the ground state, including a puckered configuration with an energy higher than the ground state by 302 cm^{-1}, and a distorted planar ring configuration, like that observed in the related tetrasilyl-substituted molecule with out-of-plane C–H bonds, that was higher in energy by 533 cm^{-1}. While these metastable configurations are different enough from the D_{2h} and D_{4h} configurations that they are unlikely to contribute to tunneling, they show that the full potential energy surface of cyclobutadiene is complex and is not harmonic with respect to deviations that break the same symmetry. This suggests that motions which break different symmetries are not completely separable.

A comparison of the vibrational frequencies between theory and experiment supports this hypothesis. As is to be expected from Fig. 3, the DFT potential well is broader and shallower than more accurate potentials used elsewhere, and this leads to an underprediction of vibrational frequencies for all excitations from the experimental values.[28] The other theoretical studies on cyclobutadiene that focus on more accurate calculations of the potential function also separate the different symmetry motions and show only a partial improvement over the work performed here.[15,16,27] This suggests that most of the remaining improvements to be made in the determination of vibrational frequencies will require us to lose the assumption that motions which break different symmetries are separable, as discussed above.

Raman excitations

Due to the tunneling and the anharmonicity, it is not immediately clear how the intensities of infra-red transitions in cyclobutadiene are to be calculated. As such, we will examine how Raman scattering can be used to probe transitions between energy levels. Transitions between nuclear vibrational energy levels will correspond directly to Raman resonances,[29,30] due to the symmetry in cyclobutadiene. The amplitude of an optical-induced transition is dependent on a transition due to the polarizability operator,[41]

$$T_{a\to b} = \langle \psi_b | \hat{P} | \psi_a \rangle, \tag{7}$$

where the transition is from nuclear vibration state a to state b, ψ_a is the wavefunction of state a, and the polarizability operator for the chosen field direction $\boldsymbol{\epsilon}$ is given by $\hat{P}_{\boldsymbol{\epsilon}} = \int d\mathbf{x}_n \, |\mathbf{x}_n\rangle \, P(\mathbf{x}_n) \, \langle \mathbf{x}_n|$, where the sum is over the permitted nuclear configurations $\mathbf{x}_n$ and $P_{\boldsymbol{\epsilon}}(\mathbf{x}_n)$ is the polarizability of the electrons for the nuclear configuration $\mathbf{x}_n$. The polarizability operator is further defined as a projection of the polarizability tensor into the field direction $\boldsymbol{\epsilon}$.

The most straightforward application of this theory to simple hydrocarbons is to make use of an approximation that the polarizability tensor changes linearly with respect to changes in the molecular configuration.[42,43] This means that in harmonic systems the transition amplitude is dependent only on the first derivatives of the polarizability tensor. Moreover, because of the linear response, the overall polarizability of the molecule can be expressed as a sum of polarizability contributions from each individual bond. However, since the polarizability is already a second-order perturbative property, even for harmonic systems, its derivative in many cases cannot be approximated as constant. Due to this and the anharmonicity, this method therefore needs to be modified in cyclobutadiene to calculate the amplitudes of Raman scattering.

We will compare the transitions from the ground state (state 0) to the two $1A_g$ states (states 2 and 3) to investigate the interaction of the Raman spectrum with the tunneling. First we must set up the basis that we will study. Motivated by previous observations that most of the wavefunction is localised near the two minima with D_{2h} symmetry, we separate the configuration space into two, these are shown by the red ovals in Fig. 10. It is necessary to use the wavefunctions of the excited vibrational states, and the only significant difference between these two wavefunctions is in their phase dependence on $\mathbf{r}_C$. The phases for the excited states are shown for our two calculation regions in Figs. 10(b) and 10(c). For the electric field, we take its orientation to be along the direction of one of the C–C bonds, as this breaks the D_{4h} symmetry in a way that permits transitions from symmetric A_{1g} to antisymmetric B_{2g} states. Finally we need the polarizability responses of the bonds to this electric field. We label the responses for C–C bonds using $T_t^{\pm}$, where T has a value of either L for long bonds or S for short bonds, t describes the orientation of the electric field $\boldsymbol{\epsilon}$ to the bond (either parallel or

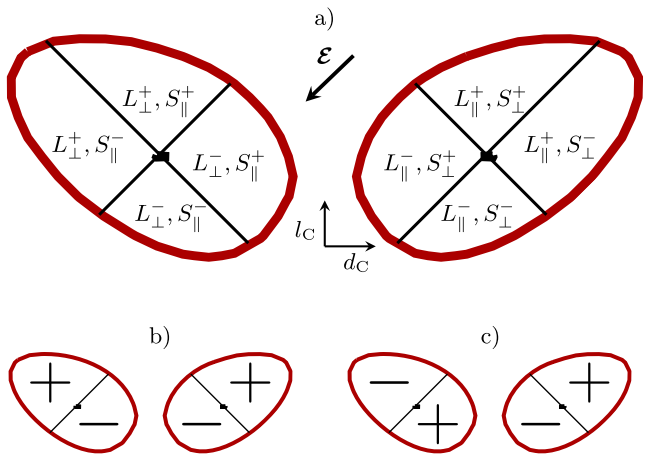

FIG. 10. (a) The eight regions $(L_l^{\pm}, S_s^{\pm})$ that can be used to determine Raman excitations to the principal excited states, and maps of the sign of the phase in (b) the symmetric $1A_g$ excitation and (c) the antisymmetric $1A_g$ excitation.

perpendicular), and ± describes the configuration of the bond which is either stretched (+) or compressed (−). With this labeling, we are able to distinguish eight distinct sub-regions that contribute to the polarizability calculation and these are shown in Fig. 10(a).

With this basis set, we are able to calculate the transition amplitude in terms of these sub-regions of the configuration space. If we define the sub-region polarizability as

$$P(L_l^{\pm}, S_s^{\pm}) = \int_{(L_l^{\pm}, S_s^{\pm})} \mathrm{d}\mathbf{r}_{\mathrm{C}} \int \mathrm{d}\mathbf{r}_{\mathrm{CH}} \langle \psi_3 | \mathbf{r}_{\mathrm{C}}, \mathbf{r}_{\mathrm{CH}} \rangle \times \hat{P}(\mathbf{r}_{\mathrm{C}}, \mathbf{r}_{\mathrm{CH}}) \langle \mathbf{r}_{\mathrm{C}}, \mathbf{r}_{\mathrm{CH}} | \psi_0 \rangle, \tag{8}$$

where the integral in $\mathbf{r}_{\mathrm{C}}$ is over the limits of the sub-region $(L_l^{\pm}, S_s^{\pm})$. We are then able to write the transition amplitude as a sum of the contributions of each sub-region

$$T_{0\to3} \approx \left(P(L_{\parallel}^{+}, S_{\perp}^{-}) + P(L_{\parallel}^{+}, S_{\perp}^{+})\right) - \left(P(L_{\parallel}^{-}, S_{\perp}^{-}) + P(L_{\parallel}^{-}, S_{\perp}^{+})\right) - \left(P(L_{\perp}^{+}, S_{\parallel}^{-}) + P(L_{\perp}^{+}, S_{\parallel}^{+})\right) + \left(P(L_{\perp}^{-}, S_{\parallel}^{-}) + P(L_{\perp}^{-}, S_{\parallel}^{+})\right). \tag{9}$$

This sum is approximate as we have not included the contribution from areas around the anharmonic central barrier, where the wavefunction amplitude is very small. Previous work calculated $T_{0\to3}$ to be approximately zero,[3] but that $T_{0\to2}$ was non-zero. From this, we can infer that $P(L_l^{+}, S_s^{\pm}) - P(L_l^{-}, S_s^{\pm})$ is non-zero, as the $0 \to 2$ transition is non-zero, so for $T_{0\to3}$ the contributions from each side of the barrier cancel out. Simply put, the derivative of the polarizability is symmetric with respect to a reflection about $d_{\mathrm{C}} = 0$. This is potentially unexpected, as it means that the polarizability response when the long bonds are aligned parallel to the electric field is the same as when the short bonds are aligned parallel. What can be interpreted from this is that the long and short bonds are not separable because the polarizability must be dependent on the conformation of the whole ring. This puts cyclobutadiene in the same category as long alkene chains, in which the polarizability is dependent on the interactions between bonds and cannot be isolated in individual bonds or sub-systems.[44]

The energy differences between the symmetric and antisymmetric states are about 5 meV; as a result, we expect these properties of the system to be sensitive with respect to interactions with the surrounding environment. To analyse how thermal and symmetry-breaking external potentials have an effect on the system, we divide the possible effects on the Raman spectrum of a symmetry-breaking external potential into three different classes when there is a (i) negligible, (ii) weak, or (iii) large external potential, compared to the energy splitting caused by tunneling.

When there is no external potential, there will be no localization into rectangular states. Optical excitations from symmetric to antisymmetric wavefunctions cannot be observed, and this means that the energy splitting caused by tunneling is not observable. However, if the temperature is high enough ($k_{\mathrm{B}}T \approx$ tunneling separation energy), then there is a thermal occupation of the antisymmetric pair of the ground state, and the Raman permitted transitions between antisymmetric pairs will be observable as excitations from the antisymmetric state to higher energy antisymmetric states are possible.

When the external potential is slightly larger than the lowest symmetric/antisymmetric pair energy difference, only those lowest energy states will be localized into a specific rectangular state, as these have the lowest nuclear momentum and the weakest tunneling, and a small energetic perturbation will localize them. To first order, the wavefunctions of these low energy states will be approximately, in terms of the free-state wavefunctions $\psi_{\pm} = \psi_0 \pm \psi_1$. The higher energy states will retain most of their tunneling characteristics. The ground state will completely lose its square symmetry. This localisation means that the transition amplitude $T_{0\to3}$ changes and instead is

$$T_{0\to3} \approx \sqrt{2}\left(P(L_{\parallel}^{+}, S_{\perp}^{-}) + P(L_{\parallel}^{+}, S_{\perp}^{+})\right) - \sqrt{2}\left(P(L_{\parallel}^{-}, S_{\perp}^{-}) + P(L_{\parallel}^{-}, S_{\perp}^{+})\right) \tag{10}$$

and excitations to all the high energy states will be observable, regardless of the temperature. This enhancement is reminiscent of catalysis, in which a metastable binding to another medium enables transitions to new states without the need for an increase in temperature.

When the external potential is larger than the highest symmetric/antisymmetric pair energy difference, all the energy states accessible from a ground-state transition will be localized. There will be very little tunneling across the barrier in any of the states. Due to the localization, each state has a rectangular configuration, and since all the states will be strongly localised, optical excitations between the two rectangular configurations will be strongly suppressed. Additionally at temperatures high enough to cause transitions between the two low energy rectangular states, tunneling effects will not be found since tunneling is suppressed for all states. Instead, depending on the exact form of the external potential, there may be vibrational differences between states, in which either the long or short bonds are aligned parallel to the gradient of the potential.

CONCLUSION

In general, tunneling is important in many chemical reactions[14,22,45] and structural phenomena. While tunneling in one dimension is easy to calculate, the extension to a multidimensional system like a coupled molecule represents a significant challenge.[46] A method of reducing this complexity is to choose a suitable tunneling pathway.[22,47] In cyclobutadiene, as in ammonia,[38] the tunneling of particular states is sensitive to the distribution of momentum. The effect of this is that particular vibrational states tunnel through the barrier along different paths, and so the calculation space must include these different tunneling routes. The rates of tunneling reactions that proceed via an adiabatic pathway are therefore dependent on eigenstates of the nuclear motion and their momentum distribution. We have shown that in some cases these can be understood as anharmonic extensions of the well understood harmonic resonance approximation that is used to classify the resonances.[29,30] This means that the nuclear motions under the well-known harmonic approximation can be used to qualitatively understand the rates and pathways of tunneling reactions, despite the multidimensional complexity of the problem.

Calculations performed here show that the square symmetry of cyclobutadiene is due to quantum tunneling, comprising correlated nuclear motion through an energetic barrier. This tunneling leads to a small correction in the energies of the vibrational frequencies of the molecule calculated under an assumed rectangular symmetry. Each energy level separates into a symmetric and an antisymmetric pair, and by analogy to the 1D double well potential, the size of the energy separation between these symmetric and antisymmetric pairs is related to the tunneling rate across the barrier. From a comparison of the different vibrational states, we find that the tunneling rate across the barrier is sensitive to the distribution of momentum in the molecule and the correlations between the motions of the nuclei. Our expectations about the motion of the molecule, for example, tunneling suppression in the out-of-phase waggle state, are able to give an accurate account of the strength of the tunneling process. We also find that despite the overall square symmetry a combination of square and rectangular labels is most appropriate to classify the dominant system excitations and the Raman spectrum. This is because the square potential is so anharmonic that the usual assumption, that at the symmetry point there is an energetic minimum, fails. Instead the global energetic minima are at points that have a rectangular symmetry. The tunneling effects are sensitive to an external potential, and a small external interaction can enable transitions to states that would otherwise be forbidden without a thermal excitation, while a large external interaction will again suppress that transition. This process is reminiscent of catalysis activation and over-binding, where a catalyst suppresses a reaction by trapping the reactants in a bound state. We have demonstrated that this method of calculating wavefunctions and energies can incorporate and enable the analysis of many complex quantum mechanical phenomena under a single approach. Perhaps more importantly, it can successfully inform our qualitative understanding and intuition about molecular motion as it generates quantitative results.

ACKNOWLEDGMENTS

This work was funded by EPSRC Grant Nos. EP/N024028/1 and EP/P022782/ and the John Templeton Foundation as part of the Durham Emergence Project. We acknowledge use of Durham Hamilton and UK Archer computer facilities.

[1] B. K. Carpenter, J. Am. Chem. Soc. **105**, 1700 (1983).
[2] R. L. Redington, J. Chem. Phys. **109**, 10781 (1998).
[3] P. Čársky and J. Michl, Theor. Chim. Acta **84**, 125 (1992).
[4] D. W. Whitman and B. K. Carpenter, J. Am. Chem. Soc. **104**, 6473 (1982).
[5] F. Fantuzzi, T. M. Cardozo, and M. A. C. Nascimento, ChemPhysChem **17**, 288 (2016).
[6] G. Maier, H.-G. Hartan, and T. Sayrac, Angew. Chem., Int. Ed. Engl. **15**, 226 (1976).
[7] R. Breslow, R. Grubbs, and S. Murahashi, J. Am. Chem. Soc. **92**, 4139 (1970).
[8] V. Gogonea, P. v. R. Schleyer, and P. R. Schreiner, Angew. Chem., Int. Ed. **37**, 1945 (1998).
[9] T. Bally, Angew. Chem., Int. Ed. **45**, 6616 (2006).
[10] A. Fattahi, L. Lis, Z. Tian, and S. R. Kass, Angew. Chem., Int. Ed. **45**, 4984 (2006).
[11] A. M. Orendt *et al.*, J. Am. Chem. Soc. **110**, 2648 (1988).
[12] B. Kovacevic, D. Barić, Z. B. Maksić, and T. Müller, J. Phys. Chem. A **108**, 9126 (2004).
[13] T. Saito *et al.*, Chem. Phys. Lett. **498**, 253 (2010).
[14] D. Ley, D. Gerbig, and P. R. Schreiner, Org. Biomol. Chem. **10**, 3781 (2012).
[15] A. Balková and R. J. Bartlett, J. Chem. Phys. **101**, 8972 (1994).
[16] M. Eckert-Maksić, M. Vazdar, M. Barbatti, H. Lischka, and Z. B. Maksić, J. Chem. Phys. **125**, 064310 (2006).
[17] A. Kostenko *et al.*, Angew. Chem., Int. Ed. **56**, 10183 (2017).
[18] Y. Shiota, M. Kondo, and K. Yoshizawa, J. Chem. Phys. **115**, 9243 (2001).
[19] P. Čársky, R. J. Bartlett, G. Fitzgerald, J. Noga, and V. Špirko, J. Chem. Phys. **89**, 3008 (1988).
[20] R. Lefebvre and N. Moiseyev, J. Am. Chem. Soc. **112**, 5052 (1990).
[21] J. Binney and D. Skinner, *The Physics of Quantum Mechanics: An Introduction* (Cappella Archive, 2010).
[22] W. T. Borden, Wiley Interdiscip. Rev.: Comput. Mol. Sci. **6**, 20 (2016).
[23] S. Coleman, *Aspects of Symmetry: Selected Erice Lectures* (Cambridge University Press, 1985).
[24] S. R. McConnell, A. Löhle, and J. Kästner, J. Chem. Phys. **146**, 074105 (2017).
[25] M. T. Cvitas and S. C. Althorpe, J. Chem. Theory Comput. **12**, 787 (2016).
[26] P. Čársky, V. Špirko, B. Andes Hess, Jr., and L. J. Schaad, J. Chem. Phys. **92**, 6069 (1990).
[27] X. Li and J. Paldus, J. Chem. Phys. **131**, 114103 (2009).
[28] B. R. Arnold, J. G. Radziszewski, A. Campion, S. S. Perry, and J. Michl, J. Am. Chem. Soc. **113**, 692 (1991).
[29] E. Wilson, J. Decius, and P. Cross, *Molecular Vibrations: The Theory of Infrared and Raman Vibrational Spectra*, Dover Books on Chemistry Series (Dover Publications, 1955).
[30] G. Herzberg, *Molecular Spectra and Molecular Structure. Volume 2: Infrared and Raman Spectra of Polyatomic Molecules* (D. Van Nostrand Company, Inc., 1945).
[31] K. V. Fernando and B. N. Parlett, Numer. Math. **67**, 191 (1994).
[32] B. N. Parlett and I. S. Dhillon, Linear Algebra Its Appl. **309**, 121 (2000).
[33] E. Anderson *et al.*, *LAPACK Users' Guide*, 3rd ed. (Society for Industrial and Applied Mathematics, Philadelphia, PA, 1999).
[34] S. J. Clark *et al.*, Z. Kristall. **220**, 567 (2005).
[35] W. Kohn and L. J. Sham, Phys. Rev. **140**, A1133 (1965).
[36] E. Silberman and H. W. Morgan, *Use of Group Theory in the Interpretation of Infrared and Raman Spectra* (Oak Ridge National Laboratory, TN, 1977).
[37] C.-K. Lin, H.-C. Chang, and S. H. Lin, J. Phys. Chem. A **111**, 9347 (2007).
[38] A. G. Csaszar and T. Furtenbacher, Phys. Chem. Chem. Phys. **18**, 1092 (2016).
[39] H. Xu, S. Saebo, and C. U. Pittman, Struct. Chem. **25**, 635 (2014).
[40] Y. Apeloig, Science **331**, 1277 (2011).
[41] M. Born and K. Huang, *Dynamical Theory of Crystal Lattices* (Clarendon Press, Oxford, 1954).
[42] D. A. Long, Proc. R. Soc. A **217**, 203 (1953).
[43] K. Gough, J. Chem. Phys. **91**, 2424 (1989).
[44] H. S. Smalø, P.-O. Åstrand, and L. Jensen, J. Chem. Phys. **131**, 044101 (2009).
[45] P. R. Schreiner, J. Am. Chem. Soc. **139**, 15276 (2017).
[46] V. Benderskii, D. Makarov, and C. Wight, *Chemical Dynamics at Low TemperaturesAdvances in Chemical Physics* (Wiley, 1994).
[47] R. P. Bell, *Experimental Evidence for Tunnelling in Chemical Reactions* (Springer US, Boston, MA, 1980), pp. 106–144.